HERA-B 00-020 RICH 00-006

Performance of the HERA-B *RICH*

D. Dujmic, R. Eckmann and R.F. Schwitters
Department of Physics
University of Texas at Austin

February, 2000

Abstract

Performance characteristics of the HERA-B *RICH* are studied with data taken during standard triggered running during the 1999 commissioning period. With the present 50-50% mixture of the design radiator gas and air, the particle identification performance is found to meet or exceed design specifications: electron-pion separation for momenta up to 15 GeV/c, pion-kaon separation to 52 GeV/c. The normalized photo-electron yield is found to be $42 \pm 5 \mathrm{cm}^{-1}\mathrm{radian}^{-2}$ and the single-photon angular resolution is better than 1 mrad. "Stand-alone" ring finding can be used to determine the direction of charged tracks in the *RICH* radiator vessel to an accuracy better than 1 mrad in vertical and horizontal angle for Čerenkov rings where at least 10 Čerenkov photons are detected.

1 Introduction

This note describes studies of the performance of the HERA-B *RICH* using data taken during 1999 for commissioning the HERA-B detector. Our goal is to understand the *RICH* performance from "first principles", using plausible analytic models for critical performance factors rather than attempting to compare myriad distributions of data with monte carlo simulations.

1.1 Čerenkov relations

The basic Čerenkov relations needed for this discussion are [1]:

$$\cos\theta_{\check{C}} = \frac{1}{n\beta} \tag{1}$$

$$\frac{dN_{\mathrm{photon}}}{dx} = \left(\frac{e}{\hbar c}\right)^2 \int dE_{\mathrm{photon}} \sin^2\theta_{\check{C}} \tag{2}$$

where n is the index of refraction of the radiator and β is the speed of the particle relative to the speed of light c. In general, n depends on the wavelength or energy $E_{\rm photon}$ of the Čerenkov photons. The indicated integral is over physical Čerenkov photons ($\cos\theta_{\check{C}} \leq 1$), weighted by the efficiencies of the *RICH* radiator, optical, and photon detector systems.

A common convention for relating the mean number of detected photons $N_{\rm photon}$ to the mean Čerenkov angle can be expressed by:

$$N_{\rm photon} = \mathcal{N}_0 T \langle \sin^2\theta_{\check{C}} \rangle \tag{3}$$

where $\mathcal{N}_0$ is a parameter that describes the overall efficiency of the detector system, T is the thickness of the radiator and $\langle \sin^2\theta_{\check{C}} \rangle$ represents the Čerenkov angle averaged over the (photon energy dependant) detection efficiency of the system. We can express $\mathcal{N}_0$ by:

$$\mathcal{N}_0 = (e/\hbar c)^2 \Delta E_{\rm photon} \quad \Delta E_{\rm photon} = \frac{1}{T}\int \eta \, dE \, dx \tag{4}$$

where η is the wavelength-dependant Čerenkov photon detection efficiency including appropriate mirror reflectivities, absorption and quantum efficiency of the PMTs. We shall call $\mathcal{N}_0$ the "normalized photon yield"; $\mathcal{N}_0$ depends on the design properties—radiator length, reflectivities of mirrors, and quantum efficiency of photon detectors—of the *RICH* system, but is *insensitive* to details of the radiator medium; it is a useful figure-of-merit for comparing different *RICH* systems. $\Delta E_{\rm photon}$ represents the photon energy acceptance of the detector system, weighted by quantum efficiency, mirror reflectivities and related efficiency factors.

We will find it convenient to express Equation 1 as:

$$\sin^2\theta_{\check{C}} = \sin^2\theta_0 - \cos^2\theta_0 \frac{m^2}{p^2} \tag{5}$$

where m is the mass of the radiating particle, p is its momentum and θ_0 is the limiting, or "$\beta = 1$" value of the Čerenkov angle, defined by:

$$\cos\theta_0 = \frac{1}{n} \tag{6}$$

In the small-angle approximation—appropriate for this application—Equations 5 and 6 simplify to:

$$\theta^2_{\check{C}} = \theta^2_0 - \frac{m^2}{p^2} \qquad \theta^2_0 = 2(n-1) \tag{7}$$

which will be used below.

The corresponding relation for photon yields—Equation 3—can be expressed in the small-angle approximation by:

$$N_{\rm photon} = \mathcal{N}_0 \, T \, \theta^2_{\check{C}} \tag{8}$$

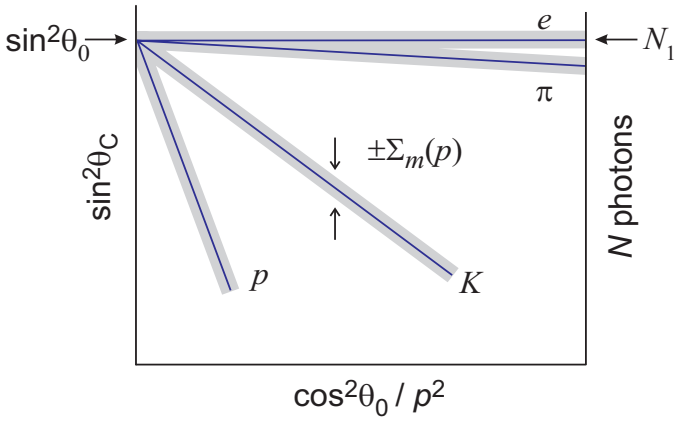

Figure 1: Schematic representation of an *r2p2* plot, where the measured values of Čerenkov angle $\theta_{\check{C}}$ and momentum p are plotted to find the particle identity through association with a particular band corresponding to a stable charged particle. Bands for electrons, pions, kaons, and protons are indicated in the figure.

1.2 The "*r2p2*" plot

The particle identification capabilities of a *RICH* are exploited by comparing measured values of the Čerenkov angle $\theta_{\check{C}}$, number of detected photons N_{photon} and particle momentum p to estimate the particle identity, which we label by its mass m. Particle identification can be visualized by plotting the measured values of $\sin^2\theta_{\check{C}}$ versus $\cos^2\theta_0/p^2$ on what we call an "*r2p2*" plot, which follows directly from Equation 5. A prototypical *r2p2* plot is shown in Figure 1

Because the average yield of photons is proportional to $\langle\sin^2\theta_{\check{C}}\rangle$ (Equation 3), the vertical scale is also proportional to the mean number of detected photons, as indicated on the right-hand axis of the figure. The mean number of photons detected on a "$\beta = 1$" track is given by $N_1 = \mathcal{N}_0 T \sin^2\theta_0$. The number of photons detected on a given Čerenkov ring also gives information on the identity of the parent particle.

It follows from Equation 5 that points from different particles will cluster into linear bands on the *r2p2* plot, the slopes of which are proportional to m^2 of the corresponding particle. Measurement errors spread the bands; projected along the $\sin^2\theta_{\check{C}}$ axis, the 1-σ error is described by $\Sigma_m(p)$ which will be estimated below.

Figure 1 demonstrates two limiting regimes for particle identification: one, the "overlap" region, at the largest values of $\theta^2_{\check{C}}$ where the different bands merge together and the second, "threshold" region where the number of detected photons vanishes. High-precision determination of the Čerenkov angle is the most important factor governing performance in the

overlap regime; photon statistics and backgrounds dominate performance in the threshold regime, effectively raising the threshold momentum of tracks above their theoretical minima. In general, particle identification strategies are different in the two regimes. In this note we concentrate on the overlap region, which puts the most stringent requirements on system performance. The ultimate threshold performance will be studied after more experience is gained with removing "background" photons associated with known Čerenkov rings from the vicinity of candidate tracks that are close to threshold.

The *r2p2* plot for tracks analyzed in this study is shown in Figure 2. Bands corresponding to electrons, pions, kaons and protons are evident. The main purpose of this note is to examine details of the observed *r2p2* plot, particularly the widths of the bands, in order to determine the performance characteristics of the HERA-B *RICH*.

1.3 Widths of *r2p2* bands

For the remainder of this note, we shall limit ourselves to the small-angle approximation, which is appropriate for case of the HERA-B *RICH*. The linear relationship between $\theta^2_{\check{C}}$ and $1/p^2$ given by Equation 7 implies that the "distance" between a given measurement point on the *r2p2* plot and a particle band is proportional to the difference, $\theta^2_{\check{C}} - \theta^2_0 + m^2/p^2$, which is simply the projection along the $\theta^2_{\check{C}}$ axis. The RMS width of a given particle band is thus described in this projection by:

$$\Sigma^2_m(p) = \delta^2(\theta^2_{\check{C}}) + 4\frac{m^4}{p^4}\left(\frac{\delta p}{p}\right)^2 \tag{9}$$

For the purposes of this discussion, where we are mainly concerned with the overlap regime, the first term in the above expression is relatively more important than the term arising from the momentum resolution, $\delta p/p$.

The resolution in Čerenkov angle has contributions from the single-photon angular resolution Δ, statistical fluctuations in the number of detected photons, and multiple-scattering of the track within the *RICH* radiator. Neglecting background photons and multiple-scattering, the resolution in $\theta^2_{\check{C}}$ is given by:

$$\delta(\theta^2_{\check{C}}) = 2\theta_{\check{C}}\frac{\Delta}{\sqrt{N_{\rm photon}}} = \frac{2\Delta}{\sqrt{\mathcal{N}_0 T}} \tag{10}$$

which is *independent* of $\theta_{\check{C}}$ and p! The two parameters, Δ and $\mathcal{N}_0$, which are sensitive to different aspects of the *RICH* design, are critical to determining its ultimate performance. Δ depends on the photon detector granularity, dispersion in the radiator gas, and optical quality of the imaging mirrors. Corrections to the ring shape and position must be made to account for

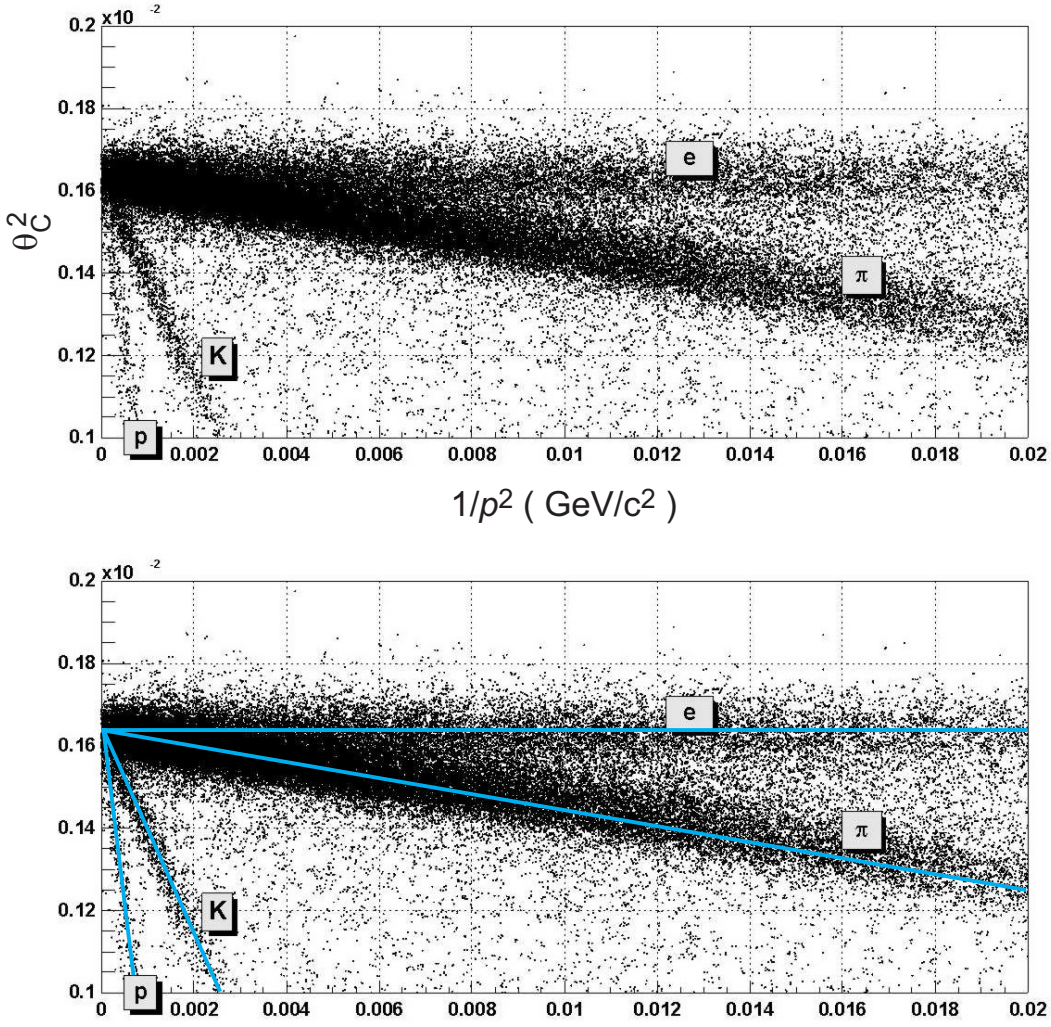

Figure 2: *r2p2* plot for the data analyzed in this study. The lower figure shows the expected positions of the electron, pion, kaon, and proton bands. The small-angle approximation is used.

spherical aberrations and other optical factors if the best resolution is to be obtained. These optical corrections are discussed in detail for the case of the HERA-B *RICH* in reference [4]. $\mathcal{N}_0$ depends on quantum efficiency of the photon detectors and light collection efficiency of the overall *RICH* system.

Multiple-scattering of the particle during its passage through the *RICH* radiator will smear the Čerenkov ring, contributing to the error in $\theta^2_{\check{C}}$ according to:*

$$\delta(\theta^2_{\check{C}})_{\rm ms} = \frac{1}{\sqrt{\mathcal{N}_0 X_0}} \left(\frac{p_{\rm ms}}{p} \right) \tag{11}$$

where $p_{\rm ms} = 13.6\,{\rm MeV/c}$ and X_0 is the radiation-length of the radiator gas. This expression should be added in quadrature to Equation 10.

The contribution of momentum errors to $\Sigma_m(p)$ depends on properties of the tracking and momentum-analysis system being used in conjunction with the *RICH*. In the present analysis, we use detected Čerenkov rings to determine the post-magnet track direction and, hence, the momentum of particles associated with Čerenkov rings. Therefore, performance characteristics of the *RICH* also enter into the momentum resolution.

The momentum resolution for magnetic spectrometers generally has the form:

$$\left(\frac{\delta p}{p} \right)^2 = A^2 + B^2 p^2 \tag{12}$$

A describes the multiple-scattering limit of the momentum resolution and B describes the measurement-error limit.

Estimates of A and B for the momentum analysis used in the present study are given in the next section.

2 Expected Performance

2.1 Photon Yield

The expected photon yield for the HERA-B *RICH* was determined by integrating Equation 3 over the relevant photon energy-dependant detection efficiencies and reflectivities. The factors included in the calculation were:

- measured reflectivities of the spherical and planar mirrors of the imaging system
- absorption (100 ppm O_2 assumed) and Rayleigh scattering in the radiator gas

*The factor of β in the multiple-scattering formula has been set to unity because all particles of interest are above Čerenkov threshold with values of β close to one.

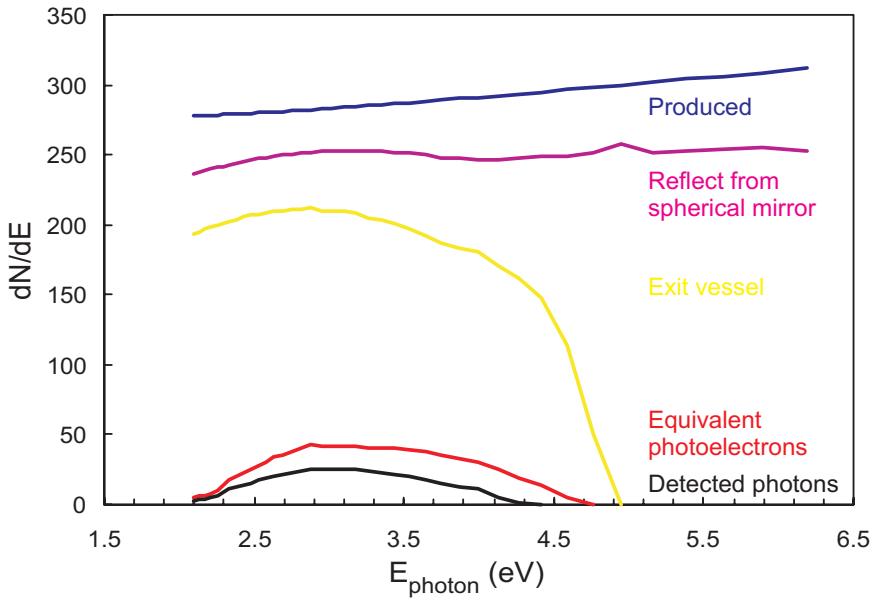

Figure 3: Differential photon yield at various stages in the HERA-B *RICH* system for pure C_4F_{10} radiator gas.

- absorption in the UVT windows of the radiator vessel using data sheets for the particular window material
- light collection efficiency, including absorption by the lens system employed in the HERA-B *RICH*
- quantum efficiency of the photomultipliers using data sheets supplied by the manufacturer

Some of these factors are indicated in Figure 3, where the differential photon yield at various stages in the *RICH* system is plotted.

Results of this integration for two radiator gasses, C_4F_{10} and N_2 are summarized in Table 1. As expected, the normalized photon yield $\mathcal{N}_0$ for complete photon rings is essentially the same for either pure C_4F_{10} or pure N_2 (or any mixture of the two). The limiting Čerenkov angle θ_0 does, however, depend on the fraction f of C_4F_{10} in the radiator vessel according to:

$$\theta_0^2 = f\,\theta^2_{C_4F_{10}} + (1-f)\,\theta^2_{N_2} \tag{13}$$

This expression can be inverted to determine the C_4F_{10} fraction in the radiator.

The values for $\mathcal{N}_0$ listed in Table 1 imply $\Delta E_{\text{photon}} \approx 0.13$ eV. This value can be understood from Figure 3 where the photon energy acceptance of the system is seen to be about 1.3 eV, implying the average detection

Radiator gas	θ_0 (mrad)	N_1	$\mathcal{N}_0$ (cm^{-1})	σ (mrad)
C_4F_{10}	52.9	36.1	46.9	0.4
N_2	23.8	7.5	48.4	0.2

Table 1: Design values for Čerenkov photon yield and angle parameters for the HERA-B *RICH*. Note that these parameters describe *complete* rings. σ is the RMS spread in Čerenkov angle for detected photons arising from dispersion in the radiator gas.

efficiency of the system is about 10%. The peak quantum efficiency of the photomultipliers is about 20% and the net reflectivity and light collection efficiency is about 50%, forming a consistent picture of the overall detection efficiency of the HERA-B *RICH*.

For reference, the HERA-B design report[2] assumed proportional-chamber-based photon detectors, claiming normalized photon yields in the range $\mathcal{N}_0 \sim 54 - 61\,\mathrm{cm}^{-1}$, which, as experience showed, was unrealistic.

The average path-length in the radiator is $T = 275$cm, which gives a yield per unit Čerenkov angle-squared $N_{\mathrm{photon}}/\theta_{\check{C}}^2 = \mathcal{N}_0 T \approx 13,000$ for complete Čerenkov rings with either of the radiator gasses listed in Table 1. Finite acceptance and shadowing by beam pipe shrouds will reduce this figure.

2.2 Single-photon angular resolution

The single-photon angular resolution Δ depends on dispersion in the radiator, detector granularity and systematic errors in the *RICH* focusing system. From Table 1, the contribution by dispersion to Δ is 0.4 mrad. The angular cell size of the M16 photomultipliers used by HERA-B is 1.6 mrad. The *RICH* mirrors were initially aligned to ± 0.1 mrad, although somewhat larger distortions to the planar mirrors were observed. Specifications on mirror quality and radius-of-curvature for the spherical mirrors were established to contribute negligibly to Δ. Optical correction algorithms were tested to reproduce the correct ring shape and track center to the 0.2 mrad level.

In aggregate, the single-photon error "budget" is:

- ± 0.46 mrad for detector granularity (M4 PMTs have twice this value)
- ± 0.4 mrad for dispersion in the radiator gas
- $\pm 0.2 - 0.3$ mrad for uncorrelated optical errors

Thus, the expected single-photon angular resolution is $\Delta = 0.7$ mrad (for M4 PMTs, $\Delta = 1.0$ mrad). The single-photon angular resolution quoted in the HERA-B technical design report[2] was $\Delta = 0.65$ mrad.

2.3 Multiple-Coulomb scattering

The radiation length of C_4F_{10} is $X_0 = 35.9\,\mathrm{gm/cm^2}$; that of N_2 is $X_0 = 38.0\,\mathrm{gm/cm^2}$. The density of C_4F_{10} is $9.94\,\mathrm{kg/m^3}$ while that of N_2 is $1.2\,\mathrm{kg/m^3}$. Thus, the number of radiation lengths represented by the *RICH* radiator is $T/X_0 = 7.6\,\%$ for pure C_4F_{10} radiator and $T/X_0 = 0.9\,\%$ for pure N_2 radiator. For most of the data described below, the radiator was an almost equal mixture of C_4F_{10} and N_2.

2.4 Momentum resolution

The momentum resolution quoted in the technical design report[2] for the HERA-B VDS and OTR tracking systems corresponds to values of the resolution parameters introduced above given by $A = 5 \times 10^{-3}$ and $B = 5 \times 10^{-5}\,\mathrm{GeV}^{-1}$; somewhat smaller values are quoted for the ITR tracking system.

Because the OTR and ITR systems are not available for the present analysis, we estimate here the momentum resolution of the VDS-*RICH*-ECAL approach used here. Briefly, we match VDS track segments, *RICH* ring centers, and ECAL clusters in the vertical (non-bend) plane to define a track. A single-point bending approximation (in the $x - z$ plane) is used to determine the momentum according to:

$$\frac{1}{p_{xz}} = \frac{\Delta\phi}{p_0} \tag{14}$$

where $\Delta\phi$ is the horizontal bend determined by the VDS and *RICH* and $p_0 \approx 650\,\mathrm{MeV/c}$ is the transverse momentum "kick" of the HERA-B dipole magnet.

The multiple-scattering limit to the momentum resolution receives contributions from three sources: 1) multiple-Coulomb scattering between the VDS measurement of track direction and the *RICH*, 2) multiple-scattering in the *RICH* radiator which blurs the observed Čerenkov ring, and 3) fringe-field effects which depend on actual trajectory through the bending magnet. These effects are described by:

$$A^2 = \frac{1}{2}\left(\frac{p_{\mathrm{ms}}}{p_0}\right)^2 \left[\left(\frac{L}{X_0}\right)_{\mathrm{trk}} + \frac{1}{N_{\mathrm{photon}}}\left(\frac{T}{X_0}\right)_{\mathrm{RC}}\right] + \left(\frac{\delta p_0}{p_0}\right)^2 \tag{15}$$

where $(L/X_0)_{\mathrm{trk}}$ represents the total material in units of radiation lengths between the VDS measurement and the *RICH*, $(T/X_0)_{\mathrm{RC}}$ is the thickness, in units of the radiation length of the *RICH* radiator gas (introduced previously), and $(\delta p_0/p_0)$ describes the fringe-field errors associated with the point-bending assumption used here. Technically, the above expression has a momentum-dependant component due to the $1/N_{\mathrm{photon}}$ factor in the

$(T/X_0)_{\rm RC}$ term which arises from the added widths of Čerenkov rings due to multiple-scattering within the radiator vessel. However, this term is negligible because: 1) $(L/X_0)_{\rm trk} \gg (T/X_0)_{\rm RC}$, and 2) multiple-scattering in the *RICH* radiator gas broadens the *width* of the Čerenkov ring with a relative contribution that is reduced by the statistical factor: $1/N_{\rm photon} \ll 1$.

We estimate $(L/X_0)_{\rm trk} \approx 1$ and $(\delta p_0/p_0) = 0.005^{\dagger}$, in which case the multiple-scattering limit of the momentum resolution is $A = 15.9 \times 10^{-3}$ for a 50-50 mixture of C_4F_{10} and N_2 as radiator. This value of A is three times worse than the design goal quoted previously; it is dominated by multiple-scattering in material between the VDS and the *RICH*.

The measurement-error limit to the momentum resolution receives contributions from the statistical error in determining the ring center that comes from detected photon statistics and from systematic errors in relating the ring center to the post-magnet track direction. We neglect errors in the VDS determination of the initial track direction and vertex position. These contributions are described by the B parameter, given by:

$$B^2 = \frac{1}{p_0^2}\left[\frac{2}{\mathcal{N}_0 T}\left(\frac{\Delta}{\theta_{\check{C}}}\right)^2 + \delta_{\rm sys}^2\right] \tag{16}$$

where $\delta_{\rm sys}$ is the systematic error in determining track directions from Čerenkov ring centers. The other quantities have been introduced previously. Assuming $\mathcal{N}_0 T = 11,500^{\ddagger}$ and $\delta_{\rm sys} = 0.5\,$mrad, $B = 8.5 \times 10^{-4}$ which is somewhat more than an order of magnitude larger than the design goal for the full HERA-B tracking system. With these parameters the momentum resolution for 10 GeV/c tracks is 1.8%.

3 Data Analysis

To the maximum extent possible, we have tried to use data acquired during the 1999 HERA-B commissioning runs to determine performance characteristics. The tools we use are: 1) tracks found in the silicon vertex tracking system (VDS) situated immediately downstream of the target wires and before the bending magnet, 2) energy clusters found in the electromagnetic calorimeter (ECAL) situated downstream of the *RICH*, and 3) Čerenkov rings found in the *RICH* which are corrected for optical aberrations to give the Čerenkov angle of the track and its post-magnet direction. Track segments, energy clusters and rings are required to have vertical angles consistent with the trajectory of a single charged track—called "matching".

Our present understanding of the critical performance parameters is presented in the following sections.

[†]Estimated from monte carlo studies of the present tracking scheme.

[‡]Reduced from 13,000 to account for partial rings.

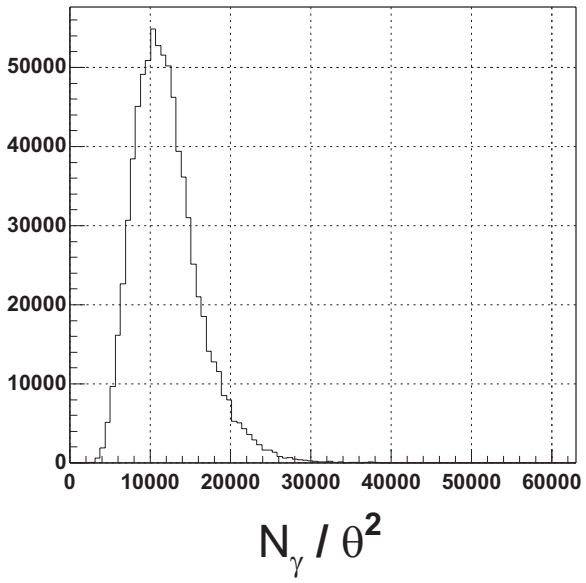

Figure 4: Histogram of $N_{\rm photon}/\theta^2_{\check{C}}$ for Čerenkov rings found by the stand-alone ring-finding algorithm for a radiator gas composed of roughly equal amounts of C_4F_{10} and N_2.

3.1 Photon yield

Measurements of the photon yield in the HERA-B *RICH* can be biased by the ring-finding algorithm, inefficiencies, and backgrounds. We have sought to understand the yield by using several approaches: 1) the results of stand-alone ring-finding, 2) "hand-scanning" rings on single-event displays, and 3) comparison with yields and occupancies calculated in monte carlo simulations. In every instance, the results are consistent with the yield estimate presented in Section 2.1, but we have not performed exhaustive studies to measure it to the %-level.

A histogram of $N_{\rm photon}/\theta^2_{\check{C}}$ for Čerenkov rings found by the stand-alone ring-finding algorithm for a radiator gas composed of roughly equal amounts of C_4F_{10} and N_2 is shown in Figure 4. The width of the observed distribution is explained by Poisson statistics. The peak value, $N_{\rm photon}/\theta^2_{\check{C}} \approx 10,000$ corresponds to $\mathcal{N}_0 = 36\ {\rm cm}^{-1}$. This distribution includes all rings found without corrections for acceptance losses or shadowing due to the beam pipe.

The scaling of $N_{\rm photon}$ with $\theta^2_{\check{C}}$ was checked by runs taken with pure N_2 as the radiator. In this case, the peak value is $N_{\rm photon}/\theta^2_{\check{C}} = 14,000$, which corresponds to $\mathcal{N}_0 = 51\ {\rm cm}^{-1}$, but is biased toward large values by the ring-finding algorithm.

An example of a "hand-scan" analysis, provided by the Ljubljana group[5]

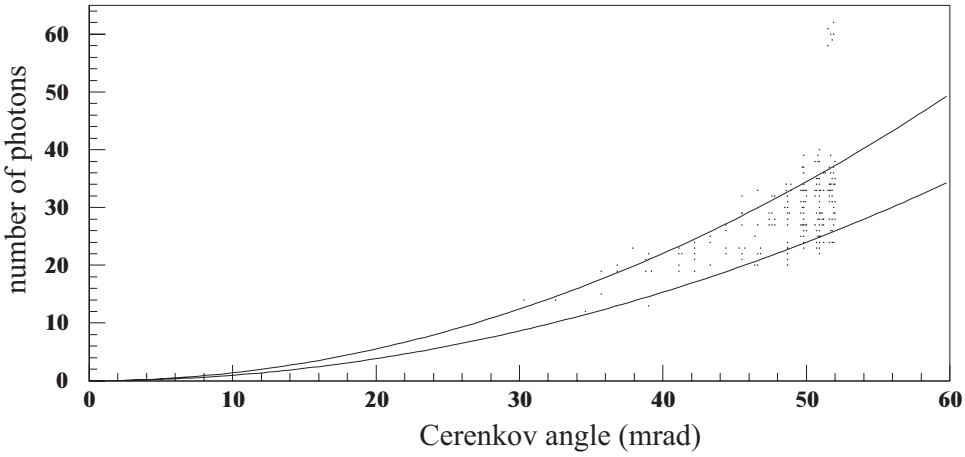

Figure 5: Histogram of $N_{\rm photon}$ versus $\theta_{\check{C}}$ for Čerenkov rings found by hand-scanning for nearly pure C_4F_{10} radiator. The cluster of points near $N_{\rm photon} = 60, \theta_{\check{C}} = 52$ mrad is due to electron-positron pairs from gamma rays converting near the entrance window of the *RICH*.

is shown in Figure 5. Their analysis determined $\mathcal{N}_0 = 43 \pm 4\,{\rm cm}^{-1}$ for the rings shown in Figure 5.

From these studies and by comparing monte carlo simulations with data, we conclude that the observed photon yield is completely consistent with expectations. To describe the yield, including acceptance losses, for a typical ensemble of Čerenkov rings, we recommend using the value $\mathcal{N}_0 = 42 \pm 5 {\rm cm}^{-1}$ or $N_{\rm photon}/\theta^2_{\check{C}} \approx 11,500$.

3.2 Single-photon angular resolution

The RMS spread in Čerenkov angle for single photons is determined directly from the data by comparing residuals for rings found by the stand-alone algorithm. Values of Δ determined for each ring found are displayed in a histogram in Figure 6. These data are consistent with the expected value $\Delta = 0.7$ mrad.

3.3 Widths of bands on the *r2p2* plot

In order to study the performance of the system, we projected the *r2p2* data along the $\theta^2_{\check{C}}$ direction as described in Section 1.3 and determined the widths ($\Sigma_m(p)$) of the projected pion and kaon bands as a function of momentum ($1/p^2$). These results are shown in Figure 7. There could be relatively small non-gaussian tails on the projected distributions that artificially increase the fitted values for widths, but these RMS values appear to fairly represent the observed widths of the *r2p2* bands.

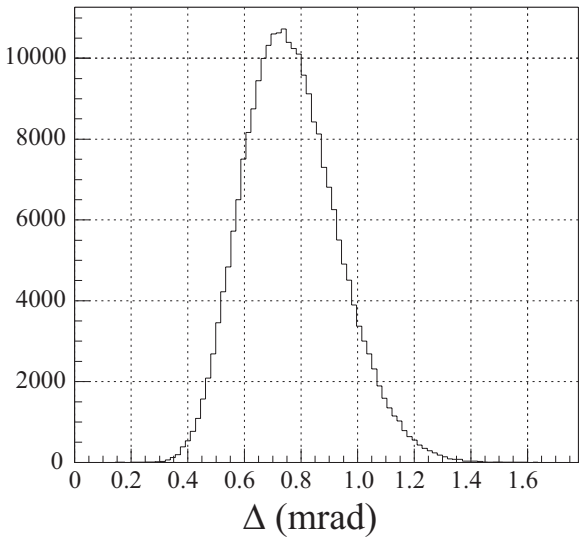

Figure 6: Histogram of the single-photon RMS angular spread for Čerenkov rings found by the stand-alone algorithm.

The resolution in $\theta^2_{\check{C}}$ is found by extrapolating bands to infinite momentum, $1/p^2 \to 0$. The result is about 50% larger than what is expected. This value can be accommodated by choosing extreme values for the key parameters: $N_{\rm photon}/\theta^2_{\check{C}} = 10,000$ and $\Delta = 1$ mrad.

At finite values of momentum, the widths of the kaon and pion bands indicate are larger than expected from our estimate of the effect of momentum resolution. The electron band, which should be essentially horizontal on the *r2p2* plot and show little momentum-dependence to its width, is even wider than the adjacent pion band (as can be seen in Figure 2). This suggests that additional errors—beyond single-photon angular resolution, photon statistics, and momentum resolution—are contributing to the widths of particle bands on the *r2p2* plot. Potential sources include: 1) larger numbers of background photons in Čerenkov rings associated with lower momentum tracks, 2) systematic errors in the Čerenkov ring-finding algorithm and 3) systematic errors in the optical corrections algorithm. The complete understanding of particle-band widths is of interest in understanding the HERA-B *RICH* performance, but the basic particle-identification capabilities of this instrument are determined mainly by the high-momentum resolution in $\theta_{\check{C}}$ (overlap region) and by the normalized photon yield (threshold region).

To better understand the effect of momentum resolution on widths of particle bands, in the next sections, we independantly determine the momentum resolution for the present tracking algorithm by examining the measured width of the $K^0_{\rm s}$ peak in $\pi^+ - \pi^-$ invariant mass spectrum and by examining the resolution in vertical (non-bend plane) angle track-matching.

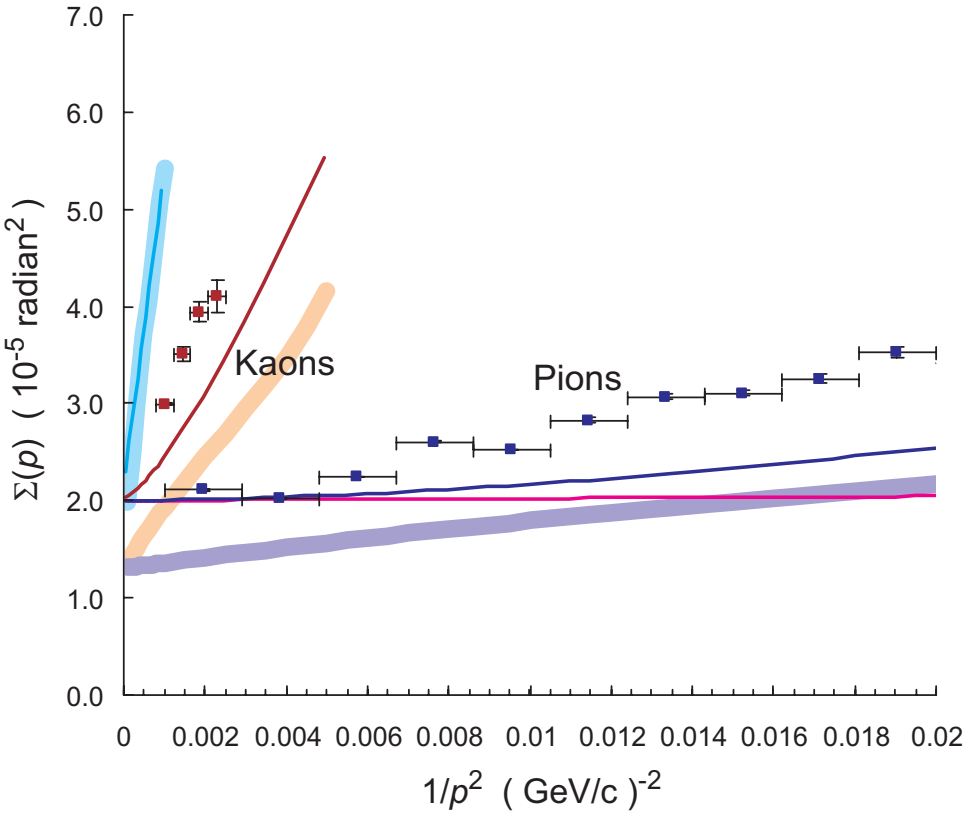

Figure 7: Resolution $\Sigma_m(p)$ on the *r2p2* plot projected in the $\theta^2_{\check{C}}$ direction. Fitted RMS widths for observed pion and kaon bands are indicated by the data points. Solid lines represent our model of the resolution for electrons (magenta), pions (dark blue), kaons (brown) and protons (cyan) using parameters chosen to describe the $p \to \infty$ limit of $\Sigma_m(p)$, the measured momentum resolution and the observed vertical angle resolution (Section 3.5 gives the parameters used for these curves.). Lightly colored bands indicate the resolutions for pion, kaon, and proton bands expected from the calculations presented in Section 2.

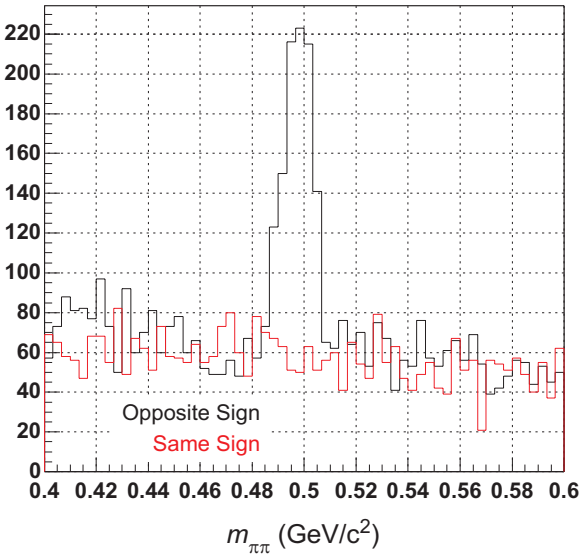

Figure 8: Invariant mass for pion pairs reconstructed using the VDS and *RICH*. Data indicated by the black lines are for opposite sign charges; red lines indicate same-sign charges. Pairs are required to have a vertex downstream of the target wire. Pairs that form a vertex at a target wire show no K^0_s peak.

3.4 Width of the K^0_s mass peak

Figure 8 gives histograms of the measured $\pi - \pi$ invariant mass spectrum for opposite-sign and like-sign pairs. A clear K^0_s signal is present for opposite-sign pairs with vertices downstream of the target wires. The RMS width of the K^0_s peak is $5.7 \pm 0.4\,\mathrm{MeV/c^2}$ (well centered on the K^0_s mass) which implies an average momentum resolution of $\delta p/p = 2.0 \pm 0.2\%$, in reasonable agreement with the estimates given in Section 2.4 for the tracks making up this peak which have typical momenta in the range $p \sim 10 - 15\,\mathrm{GeV/c}$.

Systematic errors in determining momenta could be a source of broadening of particle bands if, for example, they were charge-dependant. To study this possibility, we examine deviations from the straight-line relationship (Equation 7) of the centroid position (in $\theta^2_{\tilde{C}}$) of the pion band in Figure 2 versus momentum ($1/p^2$) separately for positively and negatively charged tracks. The results are plotted in Figure 9. While there may be some systematic charge-dependant effect, the data indicate that any global misalignment is less than 0.1 mrad, too small to account for the broader-than-expected bands. There does seem to be, however, a small systematic error in the slope of the pion band, which may be related to the large *r2p2* widths discussed above. It seems unlikely that such a possible slope error can be due to an incorrect momentum calibration because the fitted value

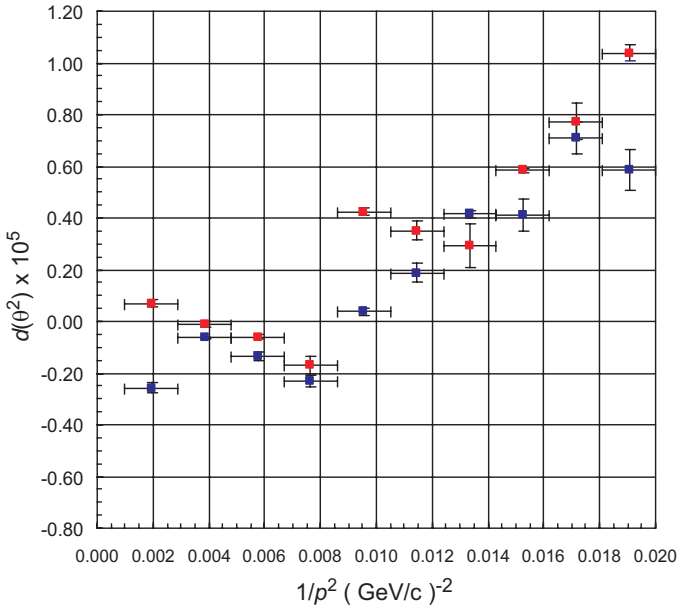

Figure 9: Deviation of centroid location (projected on $\theta^2_{\check{C}}$) of the pion band versus $1/p^2$ for positive (dark blue) and negative (red) tracks.

of the $K^0_{\rm s}$ mass agrees with the PDG value to better than 0.1 %.

3.5 Multiple-Coulomb scattering

As has been stressed, the angular resolution and photon yield of the *RICH* are the most important characteristics for determining performance. We can check the angular resolution of the *RICH* for tracks by examining the match in the vertical (non-bending) angle between the VDS and *RICH* track candidates. As before, we assume perfect resolution for tracks found by the VDS. To ensure good tracks, we take candidates from the pion band of the *r2p2* plot. The data for different momentum bins are fitted to a gaussian to determine the vertical-angle (λ) resolution σ_λ as a function of momentum. The data are plotted in Figure 10.

Using the nomenclature developed above, the resolution in vertical angle is expected to be described by:

$$\sigma^2_\lambda = \frac{2}{\mathcal{N}_0 T}\left(\frac{\Delta}{\theta_{\check{C}}}\right)^2 + \frac{1}{2}\left(\frac{p_{\rm ms}}{p}\right)^2\left(\frac{L}{X_0}\right)_{\rm trk} + \delta^2_{\rm sys} \qquad (17)$$

where the multiple-scattering contribution to the Čerenkov ring width has been neglected for the reasons discussed earlier.

Thus, a measurement of σ_λ is sensitive to some of the same critical parameters that affect the momentum resolution when matching tracks between VDS and *RICH*. The data in Figure 10 can be well described by the

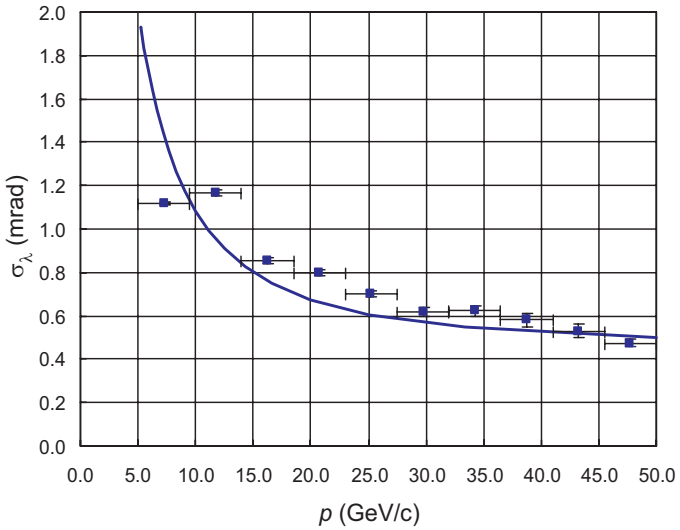

Figure 10: Resolution in vertical angle difference for pion tracks matched by the VDS and *RICH*. The solid curve is a model of the expected resolution based on parameters described in the text.

above equation with the *same* photon yield and resolution parameters used to describe the $p \to \infty$ widths of bands on the *r2p2* plot ($N_{\rm photon}/\theta^2_{\check{C}} = 10,000$, $\Delta = 1$ mrad) and with $(L/X_0)_{\rm trk} = 1.5$, $\delta_{\rm sys} = 0.2$ mrad). Note that these data suggest that somewhat more material has been placed between the VDS and *RICH* than was assumed above (Section 2.4). These parameters are in good agreement with the momentum resolution deduced above for the VDS-*RICH* tracking system based on the measured width of the $K^0_{\rm s}$ mass peak.

4 Conclusions

The HERA-B *RICH* is performing well. The two most critical parameters governing performance are essentially within design specifications and are close to the expected ultimate performance.

The normalized photon yield is in the range $\mathcal{N}_0 = 42 \pm 5\ {\rm cm}^{-1}$ which corresponds to $N_{\rm photon}/\theta^2_{\check{C}} = 11,500 \pm 1500$. This is in good agreement with the value expected for complete Čerenkov rings, accounting for shadowing and acceptance losses. Current understanding of the widths of particle bands on the *r2p2* plot suggest the lower limit of the normalized yield may be appropriate for describing the full system at present.

The single-photon angular resolution is in the range $\Delta \sim 0.7 - 1.0$ mrad. While there are indications that the resolution is at the expected level of 0.7 mrad, the widths of particle bands on the *r2p2* plot suggest that the larger

value, $\Delta = 1$ mrad, should be used to describe overall system performance as it is currently understood.

The biggest surprise is that the low-momentum limit of the *r2p2* resolution is worse than what was expected. This cannot be due to poor momentum resolution because the measured mass resolution of reconstructed K_s^0's and the observed vertical-angle resolution are consistent with expectations. Monte carlo simulations also show broader bands which implies that our estimate of resolution on the *r2p2* plot is incomplete.

Nevertheless, the particle identification capabilities of the current HERA-B *RICH* system are promising. We take present system parameters from the analysis of the preceeding section, $\mathcal{N}_0 = 37\,\mathrm{cm}^{-1}$, $\Delta = 1$ mrad , $A = 0.019$, $B = 0.00062\,\mathrm{GeV/c}^{-1}$, $\theta_0 = 40.45$ mrad (50% C_4F_{10}), to estimate the particle-identification performance. Let p_{10} be the momentum for which a given particle type will have a mean number of detected photo-electrons greater than 10. From the studies presented here[§], p_{10} represents a reasonable lower bound on the momentum for which positive identification of a track can be made by finding the associated Čerenkov ring. The upper limit on momentum for which positive identification can be made is determined by the merging of particle bands for small values of $1/p^2$. We suggest that a reasonable definition of "merging" is when the 2-standard deviation contours of adjacent bands cross at some value of momentum, p_{a-b}, where $a-b$ refer to the particle bands in question. Thus, the momentum range over which a given particle type can be positively identified is $p_{10} < p < p_{a-b}$; particle identification can be effected over larger ranges of momentum by employing other identification strategies, such as a "threshold" test for the absence of photons when $p < p_{10}$ or when other detector information is available to provide identification, such as the ECAL for $e - \pi$ separation, for example.

The methods developed in this note can be used to estimate p_{10} and p_{a-b} for the hadrons of interest in HERA-B, namely charged pions, charged kaons and protons. We have done so for the present—worst case—parameters, for the present system when the radiator is filled with pure C_4F_{10} and for the "ultimate" performance, when the estimated values for the critical parameters discussed above are achieved. These results are presented in Table 2.

From the table, it is seen that we have already met the HERA-B design goal[2] of providing $\pi - K$ identification/separation over the momentum interval 5 – 50 GeV/c. When the radiator is filled with pure C_4F_{10}, the p_{10} limits for all particles will be significantly lowered because of the larger number of detected photons at a given momentum. Better momentum resolution and improved normalized photon yield and single-photon angular resolution will significantly increase the momenta at which particle bands merge. We expect this will come with additional study and understanding

[§]Using the lower limit $N_{\mathrm{photon}}/\theta_{\check{C}}^2 = 10,000$, more than 10 photons are detected whenever $\theta_{\check{C}}^2 > 10^{-3}$.

Performance level	Pions $p_{10} - p_{e-\pi}$	Kaons $p_{10} - p_{\pi-K}$	Protons $p_{10} - p_{K-p}$
Current	5.5 – 15	20 – 52	37 – 83
Full C_4F_{10}	3.4 – 15	12 – 54	23 – 85
Ultimate	3.1 – 19	11 – 64	21 – 95

Table 2: Estimated particle identification performance of the HERA-B *RICH*. p_{10} is the momentum for which the mean number of Čerenkov photons is 10. $p_{e-\pi}$ is the momentum at which a point on the *r2p2* plot is simultaneously 2 standard deviations from the electron band and 2 standard deviations from the pion band ("2+2 sigma"). $p_{\pi-K}$ and p_{K-p} are the corresponding 2+2 sigma momenta for pion-kaon separation and kaon-proton separation. All momenta are given in units of GeV/c.

of the system.

Using the *RICH* in conjunction with other detector sub-systems to measure momentum is an unexpected benefit. The close match in Čerenkov ring radii for particles of opposite charge demonstrates that the global alignment of the system is already at the 0.1 mrad level or better.

References

[1] J.D. Jackson, *Classical Electrodynamics*, Second Edition, John Wyley and Sons, New York.

[2] Hera-B Technical Design Report, **DESY-PRC 95/01**, January 1995.

[3] D. Dujmic and R. Eckmann, *Software for Stand-alone RICH Reconstruction*, Hera-B Note **00-004 RICH**, January 2000.

[4] D. Dujmic, R. Eckmann and R.F. Schwitters, *Reconstruction of Photon Directions in the HERA-B RICH*, Hera-B Note **00-019 RICH**, March 1999.

[5] D. Škrk, Doctoral Thesis, University of Ljubljana, Ljubljana, June 1999.